Journal of Energy Storage 78 (2024) 110055

Contents lists available at ScienceDirect

Journal of Energy Storage

journal homepage: www.elsevier.com/locate/est

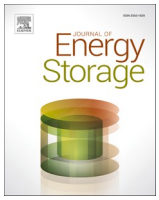

Research Papers

Technical feasibility of lined mining tunnels in closed coal mines as underground reservoirs of compressed air energy storage systems

Falko Schmidt [a], Javier Menéndez [b], Heinz Konietzky [c], Zhongming Jiang [d], Jesús M. Fernández-Oro [e,*], Laura Álvarez [f], Antonio Bernardo-Sánchez [f]

[a] Geotechnical Engineer, Santander 39011, Spain
[b] Mining and Civil Department, Sadim Engineering, Oviedo 33005, Spain
[c] Geotechnical Institute, TU Bergakademie Freiberg, 09599 Freiberg, Germany
[d] School of Hydraulic Engineering, Changsha University of Science and Technology, 410114 Changsha, China
[e] Energy Department, University of Oviedo, Gijón 33271, Spain
[f] Dept. of Mining Technology, Topography and Structures, University of León, León 24071, Spain

ARTICLE INFO

Keywords:
Closed coal mine
Energy storage
CAES
Underground reservoir
Feasibility study

ABSTRACT

In this paper, four mining levels in a closed coal mine in the Asturian Central Coal Basin (NW Spain) have been selected as a case study to investigate the technical feasibility of underground compressed air energy storage systems. First, in order to determine the suitable level and type of concrete lining, a numerical model has been established to analyze the geomechanical performance considering air pressures of 6, 10, 20 and 25 MPa and three different embodiments of concrete lining. Then, another numerical model is used to study the coupled thermo-mechanical performance at level 3, considering 100 operation cycles between 6 and 10 MPa air pressure using a circular concrete lining with a 20 mm thick sealing layer. The results obtained indicate that the deformations are lower at levels 1 and 3, where the shales are located at the top of the coal seam. Deformations and tensile stresses are significantly reduced when a circular concrete lining is used. As the thermal analysis shows, temperature fluctuations are restricted to sealing layer and concrete lining and do not reach the rock mass itself. Therefore, negligible deformations are produced by the effect of temperature compared to the effect of air pressure. Maximum tensile stress and total displacements during the operation occur at the top of the mining drift and reach 9.5 MPa and 3.6 mm, respectively. A technical feasibility can be achieved using a circular concrete lining with a suitable reinforcement system.

1. Introduction

In the transition from fossil energy production to so-called 'green energies', renewable energy production is of paramount importance. Renewable Energy Sources (RES) emit low pollutants and greenhouse gases, but have the significant disadvantage of being uncontrollable and discontinuous since they highly depend on actual weather conditions. The share of these energy sources constantly grows [1]. To ensure the stability of the electrical energy system, a balance between producers and consumers must be guaranteed all the time [2,3]. Due to the fluctuating energy production of RES, the ability to store excess energy becomes increasingly important. These storages should be of large-scale, such as Pumped Hydro Storage (PHS). Menéndez et al. [4,5] analyzed the use of abandoned coal mines in NW Spain as underground water reservoirs for PHS and presented empirical analysis and geomechanical modeling of an underground water reservoir for hydroelectric power plants. The study aims to analyze the behavior and stability of the reservoir and provides insights into its geomechanical response under different conditions. Another type of large-scale systems includes hydrogen storage facilities and Compressed Air Energy Storage (CAES) systems [6–8]. CAES systems can be implemented on the surface or underground in rock salt formations or other types of rock mass. The underground openings can be existing or newly constructed ones. This article focuses on existing ones: abandoned mines. As a positive side effect, post-mining areas can obtain new perspectives with positive local social and economic impact.

Storing fossil energy sources, hydrogen, and compressed air in underground facilities has been a research topic for decades. Due to favorable low permeability, the focus has been on rock salt caverns.

* Corresponding author.
E-mail address: jesusfo@uniovi.es (J.M. Fernández-Oro).

https://doi.org/10.1016/j.est.2023.110055
Received 23 September 2023; Received in revised form 14 November 2023; Accepted 6 December 2023
Available online 12 December 2023

Nomenclature

T_a	air temperature inside the reservoir (K)
$\dot{m}$	air mass flow rate (kg s^{-1})
t	time (s)
L	mine roadway length (m)
C_p	specific heat at constant pressure (J kg^{-1} K^{-1})
C_v	specific heat at constant volume (J kg^{-1} K^{-1})
h	heat transfer coefficient (W m^{-2} K^{-1})
T_{w1}	temperature on the sealing layer wall (K)
m_0	initial air mass (kg)
m	air mass inside the reservoir (kg)
r_1	equivalent radius of sealing layer (m)
T_0	Temperature of the air mass flow inlet (K)
P_a	air pressure inside the reservoir (Pa)
P_c	air pressure at critical conditions (MPa)
T_c	air temperature at critical conditions (K)
V	reservoir volume (m^3)
Z	compressibility factor (–)
R	gas constant (J mol^{-1} K^{-1})
f^s	shear failure envelope
σ_1	total maximum principal stress (MPa)
σ_3	total minimum principal stress (MPa)
ϕ	friction angle (°)
c	cohesion (MPa)
m_b	Hoek Brown constant for the rock mass (–)
m_i	Hoek Brown constant for the intact rock (–)
s	Hoek-Brown constant (–)
a	Hoek-Brown constant (–)
GSI	Geological Strength Index (–)
D	disturbance factor (–)
E_{mass}	rock mass deformation modulus (MPa)
E_i	Young's modulus of the intact rock (MPa)
σ_{tmass}	uniaxial tensile strength of rock mass (MPa)
σ_{ci}	uniaxial compression strength of intact rock (MPa)

Acronyms

CAES	compressed air energy storage
D-CAES	diabatic compressed air energy storage
A-CAES	adiabatic compressed air energy storage
TES	thermal energy storage
MC	Mohr-Coulomb
HB	Hoek-Brown
ACCB	Asturian Central Coal Basin
RES	renewable energy sources
ISRM	International Society for Rock Mechanics

Researchers have investigated rheological behavior, damage, and permeability changes under construction and operating conditions [9–12]. Currently, there are two operating and well-documented Diabatic Compressed Air Energy Storage (D-CAES) facilities in the world: the Huntorf plant in Germany, built in 1978, with an installed power of 320 MW using a rock salt cavern at a depth of 600 m with a volume of 310,000 m^3 and operating pressure between 4 and 7 MPa. It is capable of running at full load for 2–3 h once fully charged [13,14]. The 110 MW McIntosh plant (USA) recovers heat from the exhaust to reduce fossil energy consumption. The associated cavern, at a depth of 450 m, has a volume of 538,000 m^3 and operates between 4.5 and 7.6 MPa for up to 24 h at full load [15,16]. D-CAES plants use natural gas to raise the temperature of the outflowing compressed air, resulting in a considerable CO_2 footprint during operation. A-CAES plants store the energy from the compression load cycle and charge Thermal Energy Storage (TES) systems. This energy is later transmitted to the decompression process to condition the air for the turbine. The round-trip efficiency was evaluated for current D-CAES plants (Huntorf and McIntosh plants) considering the required fuel for the expansion process [17,18]. Ibrahim et al. [19] investigated the efficiency of A-CAES using a TES system at the inlet of the expansion process.

The use of abandoned underground mines as facilities for storing energy in form of compressed air has been investigated by Lutynski et al. [18] and Ishitata et al. [20]. Compared to underground storage caverns, CAES reservoirs are subjected to relatively high-frequency load cycles on a daily or even hourly basis. It is essential to understand the effects of high air pressure, temperature variation, and cyclic loading on the storage system. While there is good understanding of this topic in respect to rock salt, not many investigations exist for rock mass behavior of abandoned coal mines under high pressure, temperature variations, and cyclic loading. As stated by Pudewills and Droste [21] and Serbin et al. [22], in rock salt caverns, temperature has a significant influence on the creep rate, leading to large deformations and, ultimately, an effective volume loss of the reservoir. Japanese researchers presented monitoring data of a 1600 m^3 lined cavern at a depth of 450 m [20], and a 200 m^3 unlined cavern at a depth of 1000 m, tracking deformations under a pressure from 0.6 MPa down to atmospheric pressure over 5 h [23]. Rutquist et al. [24] modeled a concrete-lined rock cavern for CAES use under thermo-mechanical aspects. Khaledi et al. [25,26] showed that cyclic loading affects the stability of rock salt caverns by the development of tensile stress and crack initiation and propagation. Size and shape of the cavern have an important influence on stability. Both, stability and volume loss depend highly on the chosen operating pressure levels of CAES cavern. Damjanac et al. [27] conducted a numerical stress analysis for the 50 m high lined rock cavern in granite at Halmstad and found an increase in displacements with increasing number of load cycles. These results are confirmed by in-situ tests performed by Johansson [28] on a 9 m high shaft, 50 m deep in granitic rock. Perazelli et al. [29] documented very large deformations for CAES tunnels in weak rocks via numerical analysis in a continuous rock mass. Konietzky et al. [30] demonstrates that initial crack patterns, loading conditions, environmental conditions such as temperature, and fluid flows have an impact on the lifetime of crystalline rocks. Zhou et al. [31] indicates that the creation of tension cracks during CAES operation increases the permeability and reduces efficiency due to the loss of air. The same problem was encountered by Becattini et al. [8] with a trial cavern for an Advanced Adiabatic CAES (AA-CAES) plant constructed in a 120 m-long part of an access tunnel to the Gotthard Base Tunnel. Concrete plugs were used to isolate the high-pressure cavern from the atmosphere, and a TES was placed inside. Due to leaks in the concrete plugs, only a pressure of 7 bar (maximum system pressure is 33 bar) was achieved. An overall round-trip efficiency of 60–75 % was reached. According to the British Geological Survey (BGS), up to 100 CAES plants can be installed as salt caverns located in the Cheshire Basin (UK) [32]. According to Lutynski et al. [18], the benefits of CAES plants in abandoned coal mines are the lack of a need for new construction of openings, the restructuring of mining areas, and the promotion of green energy storage systems. Air leakage and stability assessment are challenges, as well as the distance to the existing energy grid system. Zhou et al. [31] performed a coupled thermo-mechanical simulation for an underground CAES system and found that efficiency increases with increasing injection temperature and decreasing ambient temperature. A thicker lining increases stability of the opening, but may negatively impact storage performance, and a polymer layer used for sealing has lower thermal conductivity, resulting in lower fluctuations of rock and concrete temperature. Schmidt et al. [33] analyzed the geomechanical performance of two different lining options for abandoned mine drifts: one with a 15 cm thick concrete lining and another without lining. Two 3D numerical models were

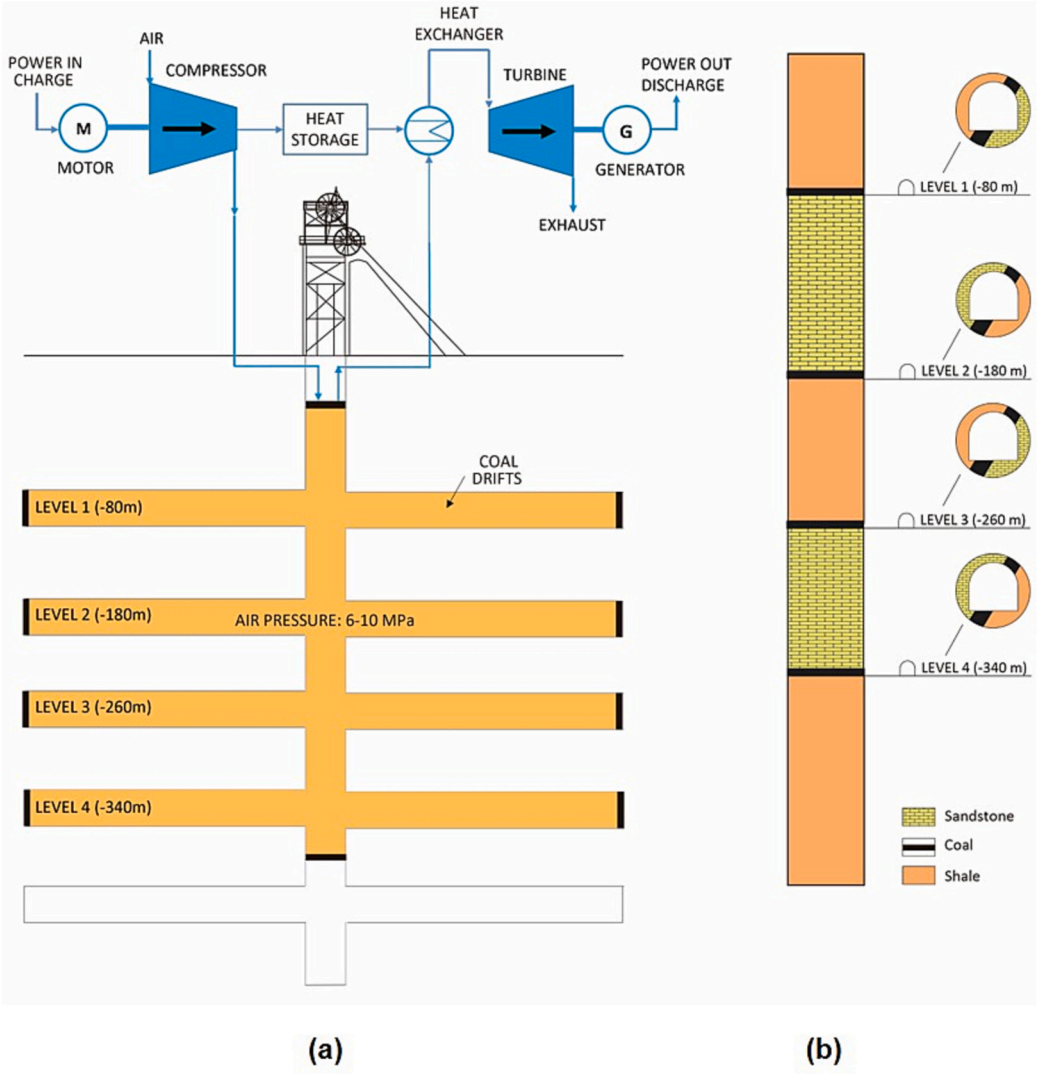

Fig. 1. (a) Schematic diagram of the adiabatic compressed air energy storage facilities and abandoned mine drifts at different levels; (b) stratigraphic column used for the numerical models.

developed to simulate the behavior of the rock mass for the entire service life, including the daily charge and discharge processes. The results suggest that the rock mass can resist the pressure with moderate deformations and small thicknesses of plastic zones, and no fatigue failure is expected during the operation time. Analytical and numerical models were developed by Alvarez et al. [34] to investigate the thermal performance of an underground reservoir considering a 50 m long mining tunnel and materials for sealing layers. They concluded that the stored energy increases when the thermal conductivity of sealing layer and rock mass increases. Menéndez et al. [35] analyzed the round-trip energy efficiency of CAES systems considering different operating conditions. They concluded that the round-trip efficiency increases when the variation of temperature inside the reservoir decreases. In addition, they also observed that the efficiency decreases when the air inlet temperature increases. The excavation damage zone was studied in a pilot lined cavern at shadow depth [36,37]. The research work concluded that air leakage and tensile fractures are reduced when the excavation damage zone is minimized. A numerical investigation was carried out by Chen and Wang [38] to investigate the stability of a mining tunnels as an underground reservoir for CAES systems. A thermo-hydro-mechanical coupled model was developed to analyze the influence of the excavation damage zone on deformation and stability of the cavern. Xu et al. [39] studied the thermo-mechanical response in an underground mining tunnel considering different construction and sealing schemes. A mine tunnel and a shaft are considered as an underground reservoir with air pressure between 4.5 and 7.58 MPa. A thermo-hydro-mechanical coupled model was conducted by Wu et al. [40] to investigate the air leakage in an unlined CAES reservoir. They concluded that the rock permeability has to be reduced essentially to reduce the air leakage during the operation of CAES systems. Jiang et al. [41] conducted a numerical and experimental analysis for a pilot lined rock cavern at shallow depth in China using a 20 mm thick fiber-reinforced plastic (FRP) as sealing layer around the compressed air. During the operation of the CAES system, they observed that the influence of the high pressure on the surrounding rock mass was limited and verified the good performance of the sealing layer employed. Menendez et al. [42] developed analytical models for A-CAES systems in lined tunnels. They considered operating pressures between 4.5 and 7.5 MPa and 0.4 m thick concrete lining and analyzed the heat transfer during the operating phase. Recently, researchers have analyzed the use of CAES systems in combination with renewable energy and hydrogen [43–47]. Lyu et al. [48] investigated the stress transfer in mining shafts structure. Kuang et al. [49] analyzed the construction of pumped storage hydropower plants in post-mining shafts. The underground water reservoirs and the powerhouse caverns would be located underground.

In this paper, a closed coal mine in the Asturian Central Coal Basin

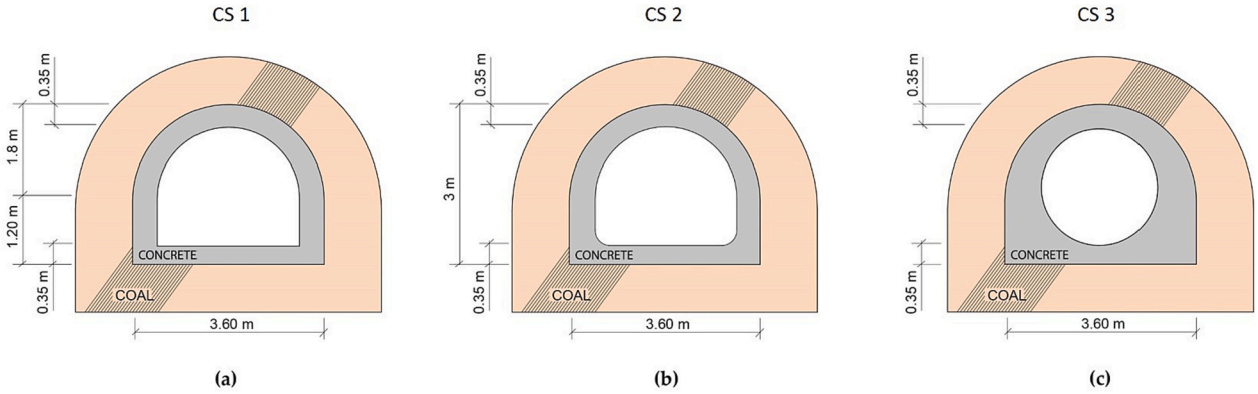

Fig. 2. Existing cross-section of mining drift and variants of concrete lining: (a) Horseshoe-shaped concrete lining; (b) horseshoe-shaped concrete lining optimized; (c) circular-shaped concrete lining.

(ACCB) is selected as a case study to investigate the technical feasibility as an underground reservoir for CAES systems. Geology and geotechnics are well known in the study area after decades of coal mining exploitation in underground mines. CAES systems are being analyzed for their implementation in the study area due to the closure of mining operations and the increase demand in energy production from renewable sources. To adapt the existing drifts to the operating conditions, concrete lining and sealing layer are required. In addition, according to the geology of the study area, shale, sandstone and a coal seams are considered in the models. Considering an adiabatic CAES (A-CAES) system, an analytical approach to obtain pressure and temperature of the stored air as input parameters for the numerical model has also been developed. Three different shapes of concrete lining with a thickness of 0.35 m are investigated: horseshoe-shaped, horseshoe-shaped optimized and circular-shaped. Time-dependence of air temperature and pressure changes of the A-CAES operation are applied to the inner surface of the lining. The impact on the surrounding rock mass, consisting of shale, coal, and sandstone, as well as the ground surface using a model with four mining levels (model A) are examined. In order to select the most appropriate mining level and concrete lining, total displacements and damage are studied in the four levels considering air pressures of 6, 10, 20 and 25 MPa. Then, according to the results obtained, a second model (model B) is used to simulate the coupled thermo-mechanical performance at Level 3 (−260 m) considering 100 operation cycles with air pressures from 6 to 10 MPa in a circular-shaped opening with concrete lining of 0.35 m thickness and FRP sealing layer. A reservoir volume of 68,000 m^3 and daily operating cycles with 8 h for charging, 4 h for expansion and 12 h for storing are considered. Temperature variations, displacements and stress field are analyzed in sealing layer, concrete lining, shale, sandstone and coal.

2. Methodology

2.1. Problem statement

The schematic diagram of the abandoned coal mine and the CAES facilities is presented in Fig. 1a. The ambient air is compressed in the compression train and the heat is stored in the TES system. Then, the air is stored in the mining drifts up to a pressure of 10 MPa. When electricity is needed, the air is released, heated in the TES and expanded in the turbines to generate electricity. Compression train, TES and turbines are installed on the surface while the compressed air reservoir is underground. In the present work, four mining levels are considered to investigate the stability of the underground reservoir in lined mining drifts. The stratigraphic column of the study area is presented in Fig. 1b. The mining drifts follow the coal seams with sandstone and shale on the top or bottom of the coal seams depending on the mining level.

First, suitable mining level and type of concrete lining must be determined. Total displacements, plastified areas and stress field are analyzed considering air pressures of 6, 10, 20 and 25 MPa. Based on the existing horseshoe mining drifts, three different options of concrete lining with a minimum thickness of 0.35 m are considered as shown in Fig. 2: a horseshoe-shaped concrete lining (Fig. 2a), an optimized shape featuring rounded corners at the bottom (Fig. 2b) and a third version with circular inner shape (Fig. 2c).

Table 1
Total tunnel length, concrete volume and surface of sealing layer for the three cross-sections considered.

Cross section	Useful cross section (m^2)	Total tunnel length (m)	Concrete lining (m^3)	Sealing layer (m^2)
CS 1	5.77	11,785	42,888	107,833
CS 2	5.70	11,929	44,250	105,101
CS 3	4.01	16,957	86,175	118,303

As documented in Fig. 2c, in case of the circular lining, the concrete thickness reaches a minimum of 0.35 m on the roof and floor areas of the drift, increasing significantly in other areas. Concrete lining has high resistance and is capable of form adapted filling of the opening in order to transmit the loads to the bedrock. In addition, the mining drifts follow the weak coal seams which surfaces have to be properly reinforced to avoid collapse, damage or leakage. A comparative analysis between the three cross sections is presented in Table 1 considering a 20 mm thick sealing layer on the inner face of the concrete lining. Tunnel length, concrete volume and surface of sealing layers are analyzed for the three types of lining. To reach a useful volume of 68,000 m^3, the length of the mining drifts is 16.96 km when cross section 3 is used. Concrete lining volume and surface of sealing layer reach 86,175 m^3 and 118,303 m^2, respectively. Note that the volume of concrete required for the circular lining (Fig. 2c) increases more than 100 % in comparison to the horseshoe lining (Fig. 2a). The proposed construction procedure is as follows: first, the installation of the corrugated steel bar reinforcement in the mining roadways is carried out. Then, a formwork system adapted to the geometry is installed and the highly resistant concrete is poured with the minimum indicated thickness. Extensive quality controls would be necessary during the construction works.

2.2. Analytical model and thermal properties

The evolution of air temperature and pressure during the operation of the CAES system has been analyzed for 100 charge and discharge cycles. The results of the analytical model have been used as boundary condition for the numerical models to investigate the coupled thermo-mechanical performance. The thermal performance of the air compressed inside the abandoned mining drifts has been resolved using a one-dimensional model developed in MATLAB. Fig. 3 shows a scheme of

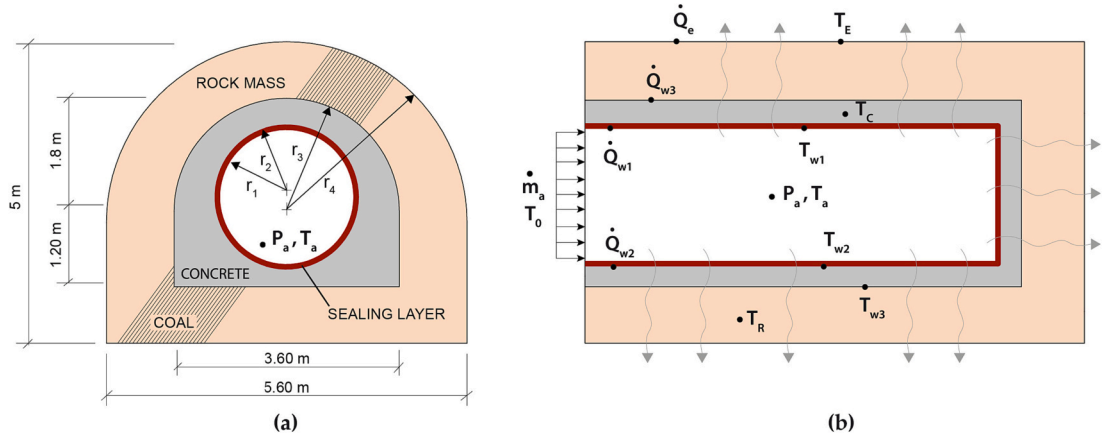

Fig. 3. Scheme of the horseshoe-shaped concrete lining tunnel used as compressed air reservoir (a) cross-section; (b) longitudinal section.

the lined tunnel with a total volume of 68,000 m^3, a total length L = 16.96 km and a useful cross-section of 4.01 m^2 (r_1 = 1.13 m, r_2 = 1.15 m), insulated with a sealing layer of 20 mm thickness. Two additional external layers (reinforced concrete lining and rock mass) are modeled to simulate the radial heat transfer towards the external regions with constant temperature of 300 K (T_E) as a boundary condition. The model resolves unsteadily the evolution of the air temperature (T_a), density (ρ_a) and air pressure (P_a) inside the reservoir as a function of the inlet (compressing at $\dot{m}_a = 100$ kg/s, $T_0 = 300$ K) or outlet (releasing at $\dot{m}_a = -180$ kg/s, $T = T_a$) mass flow rate. Daily operation cycles are considered with a duration of 8, 6, 4, and 6 h for charging, storage and expansion stages, respectively.

Application of the energy equation to the control volume occupied by the compressed air including the mass conservation to balance the inlet/outlet mass flowrates leads to the following equation system:

$$\frac{dT_a}{dt} = \frac{\dot{m}}{m}\left[\frac{C_p}{C_v}T_0 + \frac{1}{2C_v}\left(\frac{\dot{m}}{m}L\right)^2 - T_a\right] - \frac{h2\pi r_1 L}{C_v m}(T_a - T_{w1}) \quad (1)$$

$$m = m_0 + \dot{m}\, t \quad (2)$$

The unsteady solution of the system provides the temporal evolution of the air temperature inside the drift. Note that the solution depends on the instantaneous amount of trapped air (thermal properties, $C_v = 1006$ J kg^{-1} K^{-1}, $C_p = R + C_v$), as well as the heat transfer established by convection to the surrounding wall (at temperature T_{w1}). The temperature of the sealing layer is computed as a function of the external temperature, T_E, assuming lumped heat transfer by conduction through the different rock layers. More details about the complete numerical model can be found in [34]. For this study, due to the large storage volume and the wall thermal properties, a typical film coefficient of h = 50 W m^{-2} K^{-1} is adopted as representative for the convection between the air and the sealing layer [31,50]. The model has been resolved iteratively, using a backward Euler explicit discretization to resolve the coupled system of equations with a time step of 0.01 s. The computation is stopped when a maximum prescribed pressure is attained inside the reservoir (in this case ranging from 6 to 10 MPa).

In addition, the air has been considered as a real gas with a compressibility factor (Z) which is computed via the Berthelot gas state equation [34]. This formulation allows to estimate the instantaneous air pressure as a function of the temperature overtime:

$$P_a = \left(\frac{R}{V}\right) Z m T_a \quad (3)$$

$$Z = 1 - \frac{9}{128}\left(\frac{P_a}{P_c}\right)\left(\frac{T_c}{T}\right)\left(\frac{6T_c^2}{T^2} - 1\right) \quad (4)$$

T_c and P_c are air temperature and pressure at critical conditions, respectively, assumed to be 132.65 K and 3.76 MPa [34]. Additional properties for both, solid and fluid materials employed in the numerical model are listed in Table 2.

Table 2
Thermodynamic properties of air, concrete lining, rock mass and sealing layer [34,35,41].

Material	Specific heat (J kg^{-1} K^{-1})	Thermal conductivity (W m^{-1} K^{-1})	Density (KN m^{-3})	Thermal expansion coefficient (1 K^{-1})
Air	1006	0.0242	0.0117	1.0e−5
Concrete	1000	1.65	23	1.0e−5
Sandstone	950	3.50	25	1.0e−5
Shale	800	1.50	24	1.0e−5
Coal	1180	0.85	15.68	1.0e−5
Sealing layer	384	0.40	8.82	0.54e−5

2.3. Numerical modeling

2.3.1. Model geometries, meshes and boundary conditions

Numerical simulations are conducted using the FLAC3D code to assess the stability of the lined mining drifts as underground reservoirs of CAES plants [51]. FLAC3D uses the finite difference method to solve the mechanical and thermal problems in an explicit manner. The method is numerically very robust even under plastic flow and physical instabilities. Two distinct plain-strain models are developed for this analysis. Fig. 4 and Fig. 5 illustrate the geometry of these models: model A (Fig. 4a) encompasses four coal drifts located at great depths, allowing the study of high-pressure effects during operation. Model A features a free surface at the top, enabling observation of the impact on the ground surface resulting from the operation. More detailed views are presented in Fig. 4b (showcases level 2, 180 m below ground). These specific models are employed to investigate three different variants of drift lining (Fig. 4b): a horseshoe-shaped lining constructed with 35 cm thick concrete, a second variant with an optimized shape featuring rounded corners at the bottom, and a third version that adapts the lining to achieve a resulting circular inner shape. The third version introduces a variable concrete lining thickness to examine its influence on evolution of plastic zones and deformations during operation. The proposed model has an extension of 300 m by 450 m, encompassing a total of 25,200 zones. The four levels are positioned at depths of −80 m, −180 m, −260 m, and − 340 m, allowing for independent pressurization at each level. The mining drifts are situated directly within the corresponding coal seam, sandstone on one side and shale on other side depending on the level. To investigate the effects of cyclic loading, a new model for level 3,

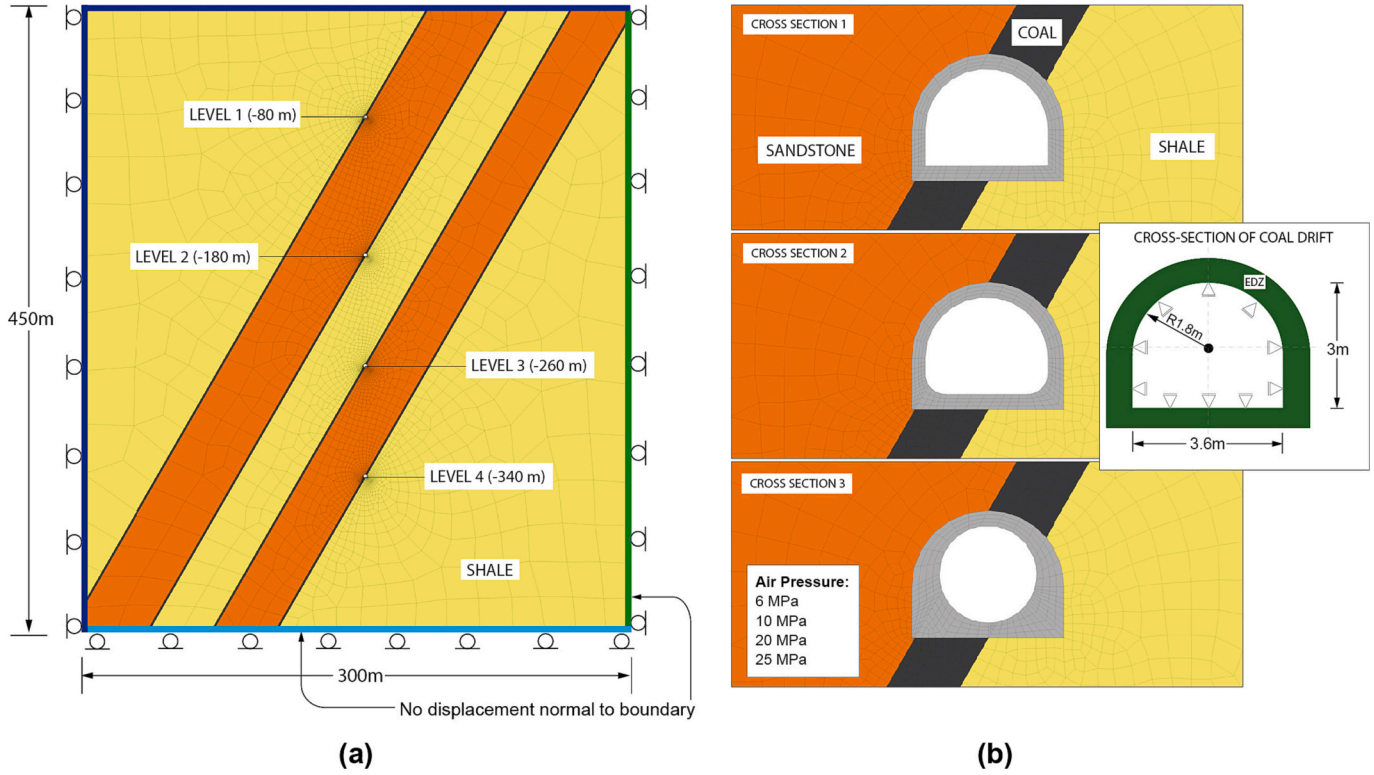

Fig. 4. Model A. (a) Geometry, mesh and boundary conditions of model A; (b) detail of the geometry of the existing coal drifts and three different concrete linings at level 2.

located at 260 m below the ground surface, is set-up. This model B (Fig. 5) has outer dimensions of 22 m in width and height. It comprises a total of 20,500 zones. The circular lining is subjected to the operating pressure of the CAES system. At level 3, the inclined shale layers reside in the upper section, while the sandstone layers are situated in the lower part. The drift intersects the coal seam between these layers. Fig. 5b illustrates the study section of Model B, where the mining drift follows a 1.5 m thick coal seam dipping 60°. To analyze the coupled thermo-mechanical response during the operation, 21 observation points are strategically placed within sealing layer, concrete lining and around the study section in the rock mass (Fig. 5c). The model also includes a 20 mm thick sealing layer. On its inner face the pressure and temperature are applied as boundary condition. Fig. 5d shows the location of the observation points in the sealing layer at the top of the drift. The study section represents the most critical area, where the geomechanical conditions are least favorable to withstanding high pressures.

Computational domains, discretization, and boundary conditions for both models are depicted in Fig. 4 and Fig. 5. The cross-section of the coal drifts is approximately 9.4 m^2. The coal drift possesses a height of 3 m and a width of 3.6 m, with a semi-circular roof, having a radius of 1.8 m. To enhance calculation accuracy, the mesh is refined in the proximity of the excavations and becomes gradually coarser towards the outer regions. In both models, roller boundaries are implemented at the bottom and along the vertical outer boundaries. On the upper boundary of model B, a vertical load of 6.5 MPa is applied, representing the weight of the overburden.

According to experience from the study area, the rock mass strength can be characterized by the Mohr-Coulomb (M-C) failure criterion [4,33]. In the conventional M-C model, it is assumed that the strength properties of the materials remain constant once plasticity occurs. This assumption implies that the material can sustain a stress equal to the failure strength even after surpassing the failure envelope. The M-C failure criterion is expressed by Eqs. (5) and (6).

$$f^s = \sigma_1 - \sigma_3 N_\phi + 2c\sqrt{N_\phi} \tag{5}$$

$$N_\phi = \frac{1 + sin(\phi)}{1 - sin(\phi)} \tag{6}$$

where f^s is the shear failure envelope, σ_1 and σ_3 are the total maximum and minimum principal stresses, respectively, ϕ is the friction angle (°) and c is the cohesion (MPa).

2.3.2. Simulation procedure

To simulate the impact of high air pressure and cyclic loading, the following procedures are applied. Initially, isotropic stress conditions are assumed ($\sigma_{xx} = \sigma_{YY} = \sigma_{ZZ}$). In model A, the initial primary stress varies between 0.0 MPa at the free surface and 11.2 MPa at the bottom of the model. As for model B, the initial primary stress is set at 6.5 MPa at the level of the drift. The in-situ horizontal stresses were estimated using empirical equations based on global data and a compilation of local data specific to the ACCB region in northwest Spain [4,5,33]. These estimations were crucial for determining the initial stress distribution within the models.

For model A, the simulation involves the following steps: (1) generation of the primary stress field: vertical and horizontal stresses are initialized, (2) excavation of the four drift levels: The process of excavating the four drift levels is simulated, replicating the actual underground excavation sequence. After that, the installation of the correspondent concrete lining is carried out, (3) application of air pressures: air pressure values of 6, 10, 20, and 25 MPa are applied, starting from the lowest level (level 4) and subsequently progressing to the next drift level above. This sequence ensured that all four pressure levels are sequentially applied to the active drifts, culminating in the final step where all four drifts are subjected to the indicated air pressures.

These aforementioned steps are executed for all three concrete lining variants. Throughout the simulation, plasticity state, stress field, as well

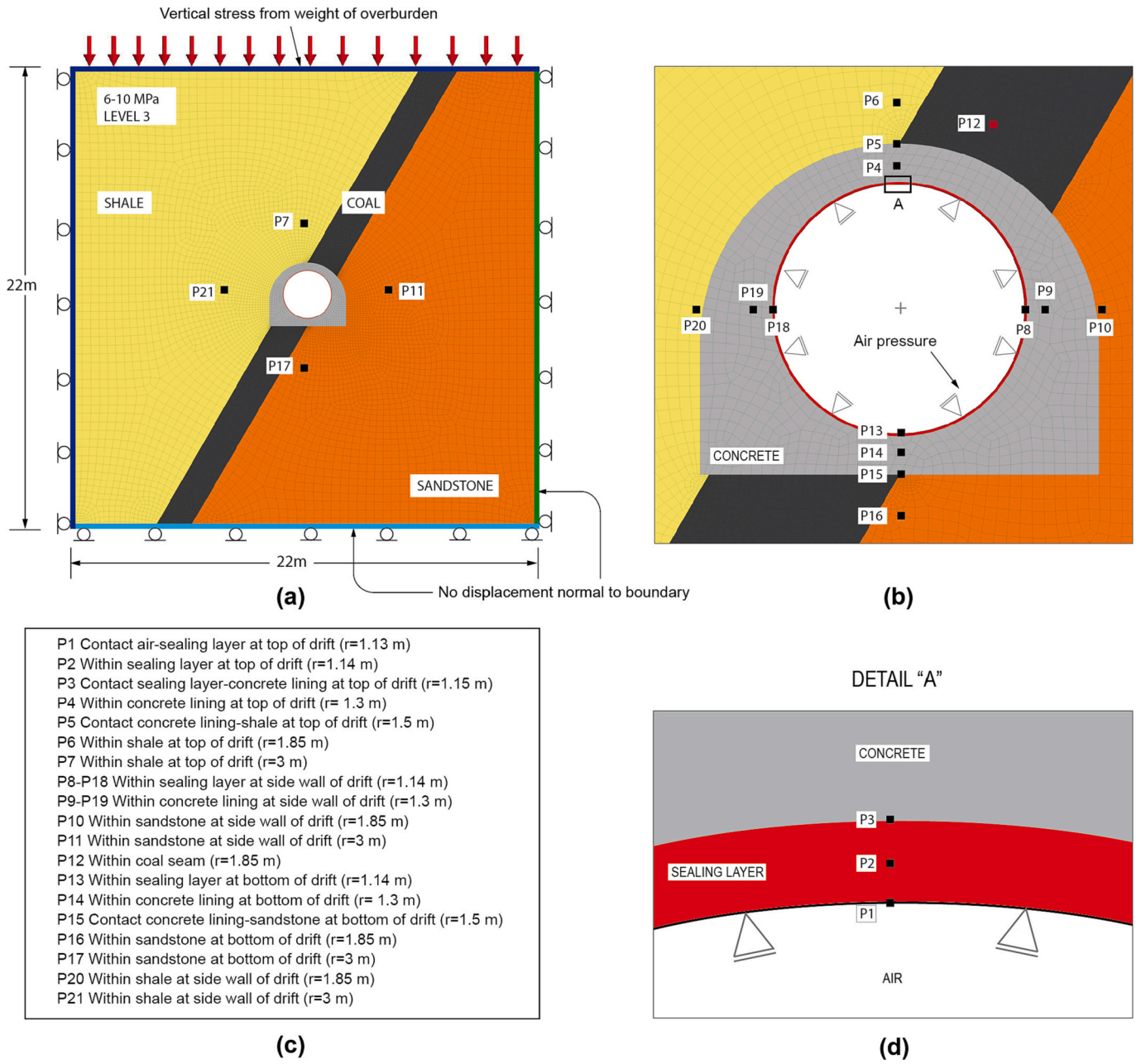

Fig. 5. Model B. (a) Geometry, materials, mesh and boundary conditions for level 3; (b) mesh details, concrete lining, sealing layer and observation points; (c) location of observation points; (d) detail of observation points in the 20 mm thick sealing layer at the top of the drift.

as deformations are monitored and analyzed. The purpose was to track and evaluate the response of the system under varying pressure conditions, providing insights into the behavior of the underground infrastructure.

In the case of model B, the simulation involves the following steps: (1) generation of the primary stress field, (2) excavation of coal mining drifts, (3) installation of circular concrete lining. Additionally, a 2 cm thick fiber-reinforced sealing is applied to the inner side of the concrete lining, (4) resetting of displacements: displacements within the model were reset to their initial positions in order to measure the effects of pressure and temperature accurately, (5) application of cyclic loads: cyclic pressures and temperatures resulting from the charge and discharge processes are applied to the inner face of the sealing layer. The applied pressures range from 6 MPa to 10 MPa during 100 operating cycles, with each complete cycle lasting 24 h, resembling the operational conditions of the CAES system. To isolate the effects of temperature and pressure, separate runs were conducted for temperature-only, pressure-only, and combined temperature and pressure variations. This separation is necessary as the influence of temperature is found to be minimal compared to the effects of pressure.

These steps are crucial in investigating the response of the system to cyclic loading, assessing the impact of pressure and temperature, and their combined effects on plasticity, displacements, and stress redistributions within the concrete lining.

2.4. Material properties

The rocks properties were determined by laboratory testing following the suggested methods of the International Society for Rock Mechanics (ISRM) [52]. Laboratory tests were performed on 40 core samples at the Mechanical Laboratory of the University of Oviedo. Unconfined compressive strength tests, Brazilian tensile tests, direct shear

Table 3
Intact rock properties, GSI and Hoek-Brown constants [4,33].

Parameter	Shale	Sandstone	Coal
Unit weight, γ (kN m^{-3})	22.68	25.87	15.00
Intact Young's modulus, E_i (MPa)	21,000	43,650	32,900
Intact uniaxial comp. strength, σ_{ci} (MPa)	35	150.8	8.0
Intact rock constant (m_i)	9.2	15.4	8.0
GSI	35	50	51
m_b	0.903	2.582	0.433
s	0.00073	0.00386	0.00059
a	0.5159	0.5057	0.5053

Table 4
Properties of rock mass, concrete lining and sealing layer [4,33,41].

Lithology	Young's modulus (MPa)	Poisson's ratio	Tensile strength (MPa)	Cohesion (MPa)	Friction angle (°)
Shale	2381	0.27	0.028	0.67	37.7
Sandstone	13,409	0.25	0.226	2.02	52.7
Coal	3200	0.32	0.010	0.25	20.0
Concrete	23,000	0.27	2.000	5.00	40.0
Sealing layer	2900	0.22	130	1.5	30

tests of discontinuities and triaxial compression tests were carried out to determine the intact rock properties. Table 3 shows the intact rock properties (unit weight, intact uniaxial compressive strength, intact Young's modulus and intact rock constant m_i), Geological Strength Index (GSI) and Hoek-Brown constants (m_b, s and a) for shale, sandstone and coal.

The Hoek-Brown parameters for the rock mass were obtained by applying Eqs. (7), (8) and (9) considering GSI and disturbance factor (D), which accounts for the extent of disruption experienced by the rock mass during the excavation phase, particularly due to blast damage. Disturbance factors of 0 and 0.8 for shale and sandstone and coal have been considered, respectively. The rock mass properties such as deformation modulus (E_{mass}) and uniaxial tensile strength (σ_{tmass}) were obtained by applying Eqs. (10) and (11), respectively. Finally, the Hoek-Brown failure criterion has been employed to obtain the equivalent M-C strength parameters (cohesive strength and friction angle) [53]. The geotechnical properties of rock mass, concrete lining and sealing layer are shown in Table 4.

$$m_b = m_i exp\left(\frac{GSI - 100}{28 - 14D}\right) \tag{7}$$

$$s = exp\left(\frac{GSI - 100}{9 - 3D}\right) \tag{8}$$

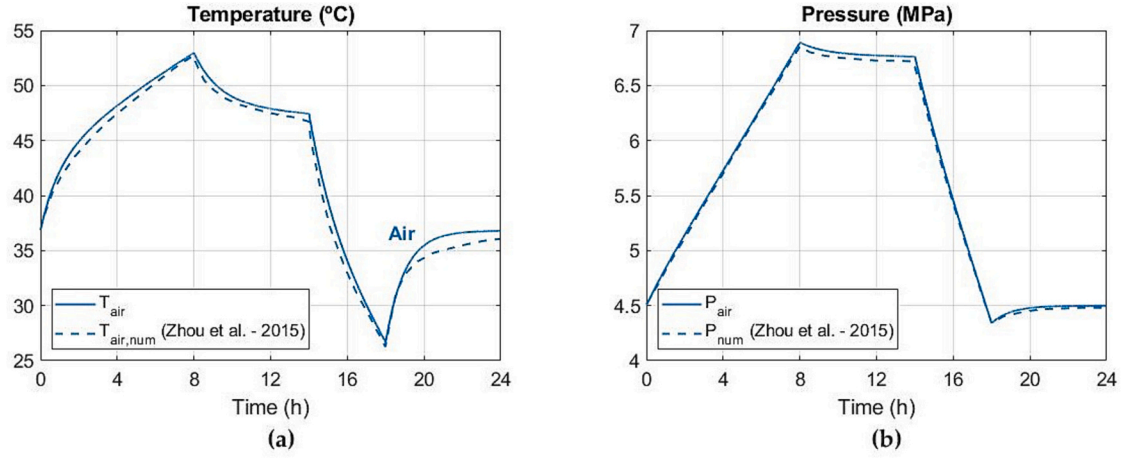

Fig. 6. Model validation. Comparison with analytical model developed by Zhou et al. [54].

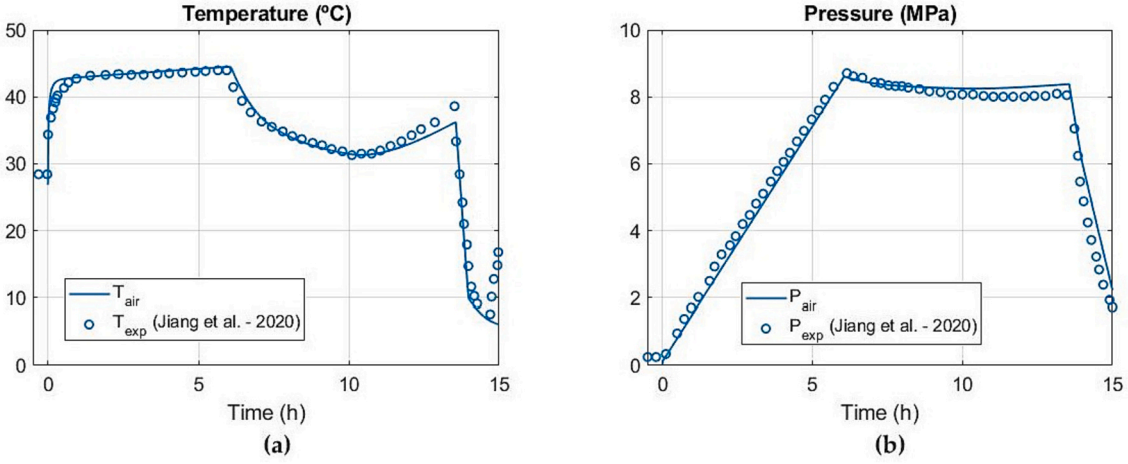

Fig. 7. Model validation. Comparison with experimental model developed by Jiang et al. [41].

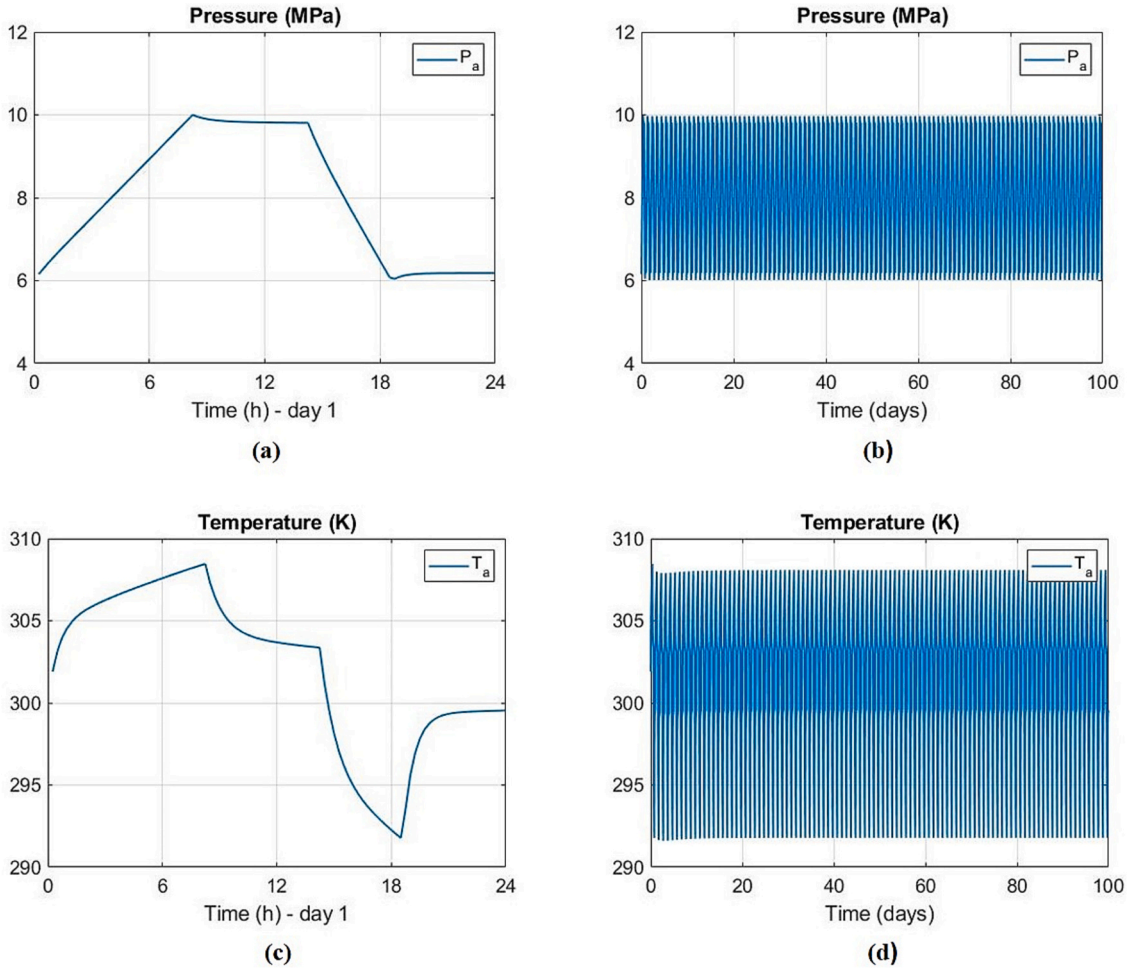

Fig. 8. Evolution of air pressure and temperature inside the underground reservoir during charge and discharge. (a) Air pressure during the first cycle; (b) air pressure during 100 operation cycles; (c) air temperature during the first cycle; (d) air temperature during 100 operation cycles.

$$a = \frac{1}{2} + \frac{1}{6}\left[exp\left(\frac{-GSI}{15}\right) - exp\left(\frac{-20}{3}\right)\right] \tag{9}$$

$$E_{mass} = E_i\left(0.02 + \frac{1 - D/2}{1 + exp^{((60+15D-GSI)/11)}}\right) \tag{10}$$

$$\sigma_{tmass} = \frac{-s\,\sigma_{ci}}{m_b} \tag{11}$$

2.5. Model validation

The results of the analytical model have been compared with other approaches provided in literature. Fig. 6 shows a comparative analysis with the analytical model developed by Zhou et al. [54]. Zhou et al. carried a coupled thermo-mechanical analysis for an operation of CAES systems in lined rock caverns. Air temperature (Fig. 6a) and pressure (Fig. 6b) are compared during the first operation cycle, reaching good agreements. In addition, to justify the accuracy of the one-dimensional thermal model, the results have also been compared with an experimental model performed by Jiang et al. [41] in a lined rock cavern at shallow depth. As shown in Fig. 7, good agreements have been obtained between the present model (solid blue lines) and the experimental model (dots).

3. Results and discussion

3.1. Analytical model

Results of the one-dimensional analytical model are presented in Fig. 8. Air temperature and pressure are used as boundary conditions for the numerical analysis. The evolution of the air pressure during the first operation cycle is shown in Fig. 8a. Daily operation cycles with 8 h of charging, 6 h of storage after charging, 4 h of discharging and 6 h of storage after discharging are considered. Air mass flow rates of 100 and 180 kg s^{-1} have been considered for charging and discharging stages, respectively, in an underground reservoir with 68,000 m^3. Fig. 8c and d show the temperature variation at the air inside the reservoir during the first cycle and 100 operation cycles, respectively. Maximum and minimum temperatures of 308 K and 292 K, respectively, are reached during operation inside the reservoir considering an inlet temperature after compression of 300 K.

3.2. Mechanical performance

In order to determine the most appropriate level and type of concrete lining, a stability analysis is carried out for the four mining levels. The lined tunnels are subjected to air pressures of 6, 10, 20 and 25 MPa considering the three variants of concrete lining. In order to analyze the behavior of the system (total displacements, plasticity and tensile stress in the concrete lining) the openings were submitted to extreme air pressures, much higher than the operating pressure. According to the

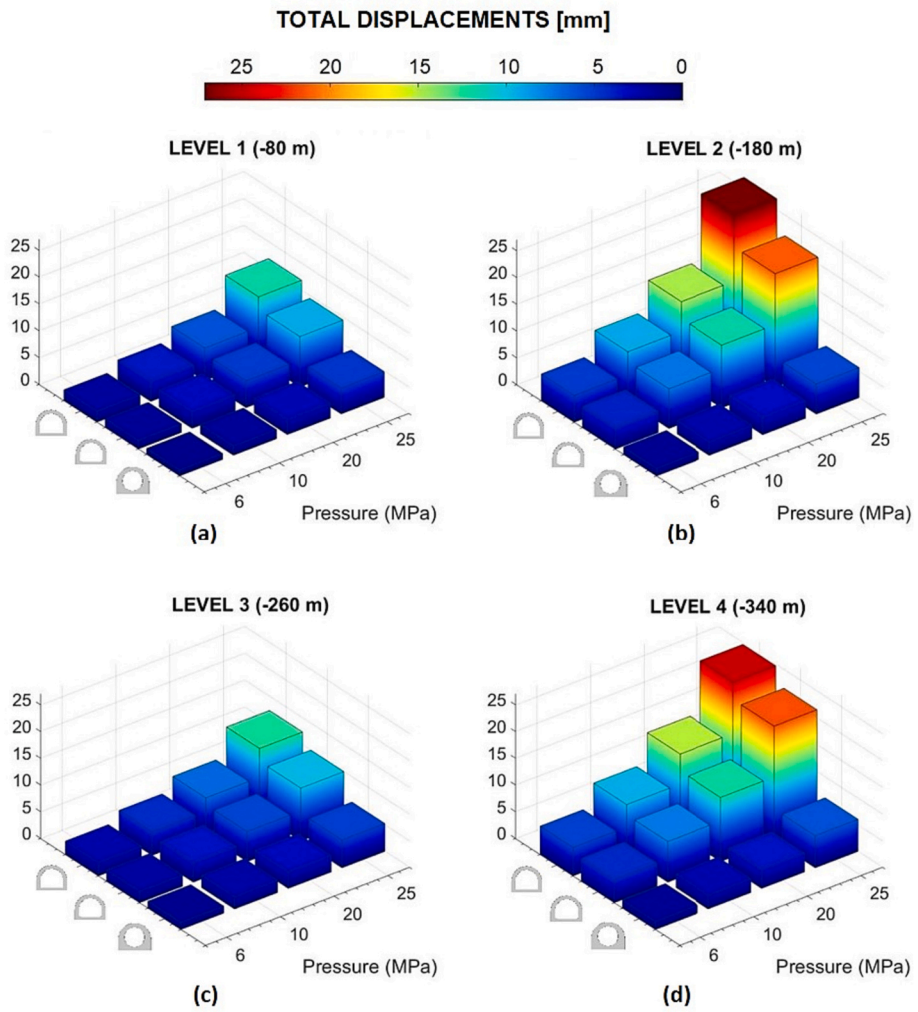

Fig. 9. Total displacements considering air pressures of 6, 10, 20 and 25 MPa and three concrete linings. (a) Level 1 (−80 m); (b) level 2 (−180 m); (c) level 3 (−260 m); (d) level 4 (−340 m).

stratigraphy, shales are located at the top of the coal seam in levels 1 and 3 and at the bottom of the coal seam in levels 2 and 4. Total displacements are shown in Fig. 9 for the three variants of concrete lining and air pressures. Smaller values of total displacements are reached in levels 1 and 3, where the shales and sandstone are located at the top and bottom of the coal seams, respectively (Fig. 9a and c). Maximum total displacements of 27.4 mm are reached at level 2 when a pressure of 25 MPa is applied and the horseshoe-shaped concrete lining is used (Fig. 9b). The displacements are reduced down to 6 mm when the circular concrete lining is used. Total displacements are significantly reduced in all cases when the circular concrete lining is used. The lowest values of deformation are obtained for levels 1 and 3. At an operation pressure of 10 MPa, total displacements reach 3.8 and 4.3 mm in levels 1 and 3, respectively, being reduced to 1.8 and 2.2 mm when using the circular concrete lining. Therefore, similar deformation results are obtained in levels 1 and 3. Level 1 is the oldest level and its current state of conservation could cause safety issues. Furthermore, the total length of drifts available at level 1 is less than those at level 3. Based on stability analysis and availability of drifts, level 3 with a circular-shaped concrete lining is selected as the most appropriate location for a CAES system.

Total displacements for level 3 are represented in Fig. 10 and Fig. 11 for the three variants of concrete lining considering air pressures of 10 and 6 MPa (operating pressure). The maximum values in the concrete lining occur at the left wall in all the analyzed scenarios. In addition, significant deformations can also be observed at the floor of the drifts. Total displacements reach 4.3 mm at an operating pressure of 10 MPa (Fig. 10a) using the horseshoe-shaped concrete lining, being reduced down to 3.6 and 2.3 mm for the horseshoe-shaped optimized and circular concrete lining, respectively. Total displacements reach 2.5 mm at 6 MPa (Fig. 11b), decreasing to 1.3 mm in the case of circular concrete lining (Fig. 11c).

Plastification type and extent in the rock mass around the mine drifts is shown are Fig. 12 for an air pressure of 10 MPa considering the three variants of concrete lining. A combination of tensile and shear plastifications is observed mainly in the left wall and the floor. The plastifications are associated with the coal seam due to its lower resistance compared to shale and sandstone. Shear and tensile failures are reduced when the circular concrete lining is employed, mainly in the floor of the drift (Fig. 12c). In this scenario, the concrete lining absorbs air pressure and reduces stresses in the rock mass. Finally, the tensile stress in the concrete lining is shown in Fig. 13 considering a maximum operating pressure of 10 MPa. The maximum value reaches 50 MPa and occurs at the left corner on the floor using the horseshoe-shaped concrete lining. Note that this high value is obtained due to the elastic behavior that has been assumed for the concrete lining. Elastic material is used for the concrete to demonstrate the effect of the liner shape on the evolution of tensile stresses. Tensile stresses decrease significantly to less than 10 MPa when circular concrete lining is employed (Fig. 13c). For the elastic concrete lining a circumferential strain of 0.006 % is expected during to the operation. This should be kept in mind for rebar design and potential

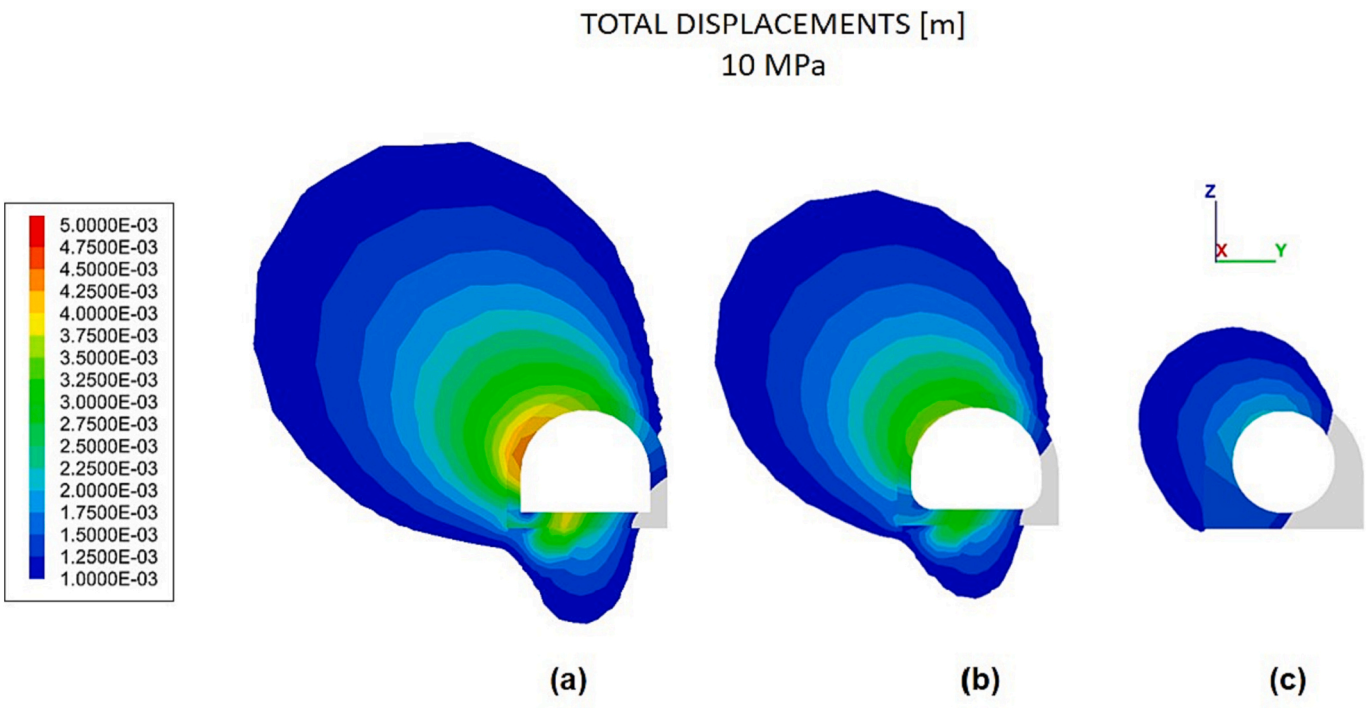

Fig. 10. Total displacements at level 3 considering an air pressure of 10 MPa. (a) Horseshoe-shaped concrete lining; (b) horseshoe-shaped concrete lining optimized; (c) circular-shaped concrete lining.

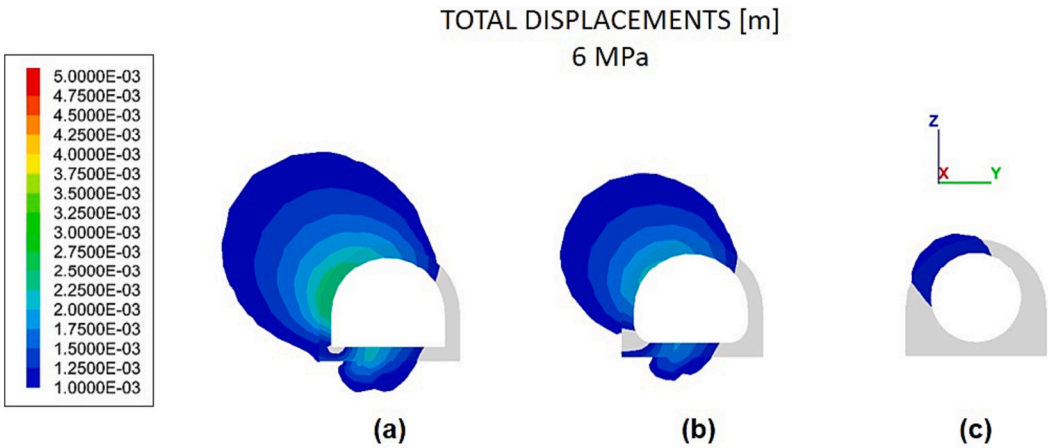

Fig. 11. Total displacements at level 3 considering an air pressure of 6 MPa. (a) Horseshoe-shaped concrete lining; (b) horseshoe-shaped concrete lining optimized; (c) circular-shaped concrete lining.

crack formation, but is not considered here.

3.3. Thermo-mechanical coupled analysis

The thermo-mechanical response of the lined drifts is investigated for level 3 (−260 m) considering cyclic loading with air pressures between 6 and 10 MPa during 100 operating cycles with an inlet temperature of 300 K. First, the effect of the temperature variations on the stability of the lined drifts is analyzed. The evolution of the temperature during charging, storage and discharging at sealing layer, concrete lining and rock mass is shown in Fig. 14. Fig. 14a shows the temperature variation at the top of the drift during the first 48 h of operation (2 cycles). Slight temperature fluctuations are observed in sealing layer and concrete lining, but nearly no temperature variations occur in the rock mass. The maximum temperature variation reaches 16 K at point P1, a contact of the sealing layer with the compressed air. At point P5 (contact surface between concrete lining and rock mass) a temperature variation of 1.5 K is obtained. The temperature fluctuates between 305.3 K and 296.5 K at point P3. The evolution of the temperature is presented in Fig. 14b for 100 operation cycles. As can be seen, the temperature variation remains constant at all points during the long-term operation of the CAES system.

The distribution of temperature in sealing layer and concrete lining is presented in Fig. 15 after 8 h compression at 10 MPa when the value is the greatest (Fig. 15a) and after 6 h expansion at 6 MPa when the value is the lowest (Fig. 15b). These two states are representative for the entire 100 cycles, since Fig. 14b shows no overall increase in temperature. During charging, the temperature of the compressed air increases and heat is transferred to sealing layer and concrete lining. As indicated previously, due to the thermal conductivity of the FRP, slight temperature fluctuations occur. Conversely, as shown in Fig. 15b, during the expansion stage the temperature of the concrete lining is higher and heat is transferred to the compressed air inside the reservoir. As shown in

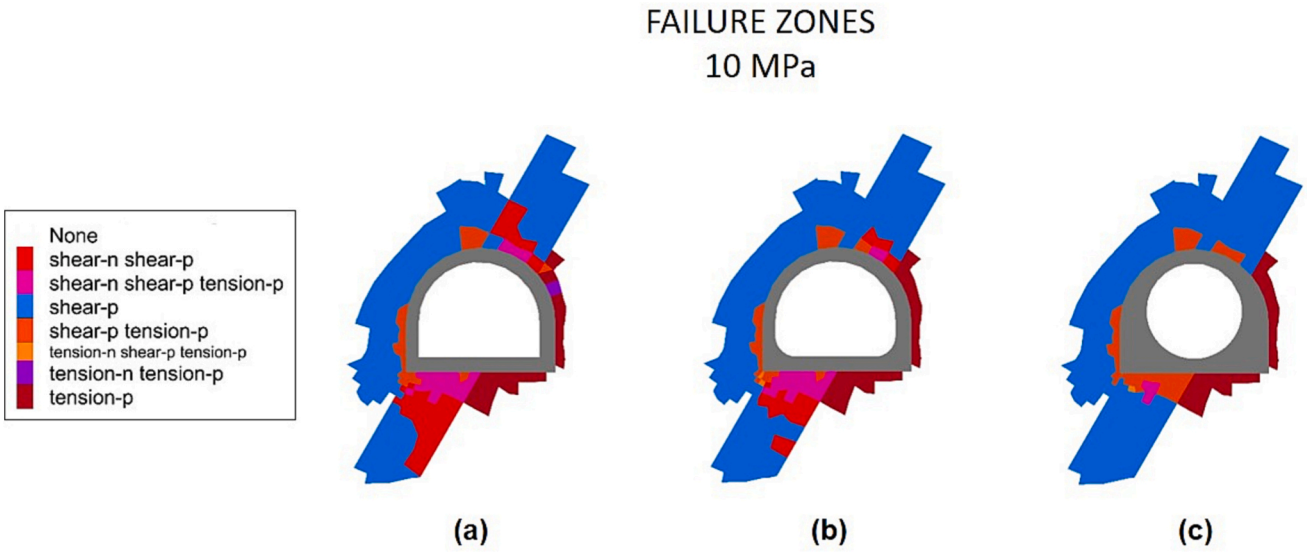

Fig. 12. Failure zones at level 3 considering an air pressure of 10 MPa. (a) Horseshoe-shaped concrete lining; (b) horseshoe-shaped concrete lining optimized; (c) circular-shaped concrete lining.

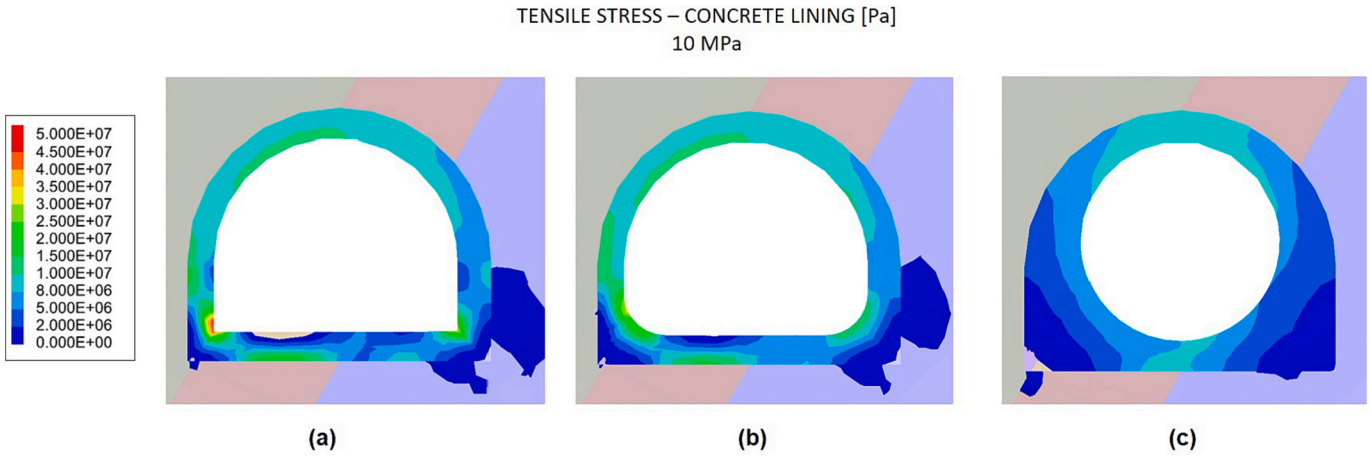

Fig. 13. Tensile stress in concrete lining at 10 MPa air pressure. (a) Horseshoe-shaped concrete lining; (b) horseshoe-shaped concrete lining optimized; (c) circular-shaped concrete lining.

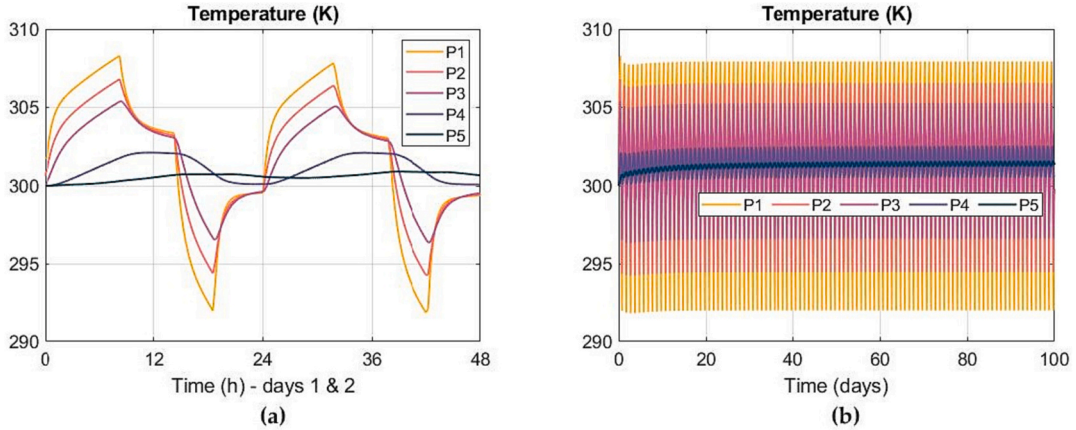

Fig. 14. Evolution of the temperature during air charge and discharge at sealing layer, concrete lining and rock mass at the top of the drift. (a) First 48 h of operation; (b) 100 operation cycles. Points P1 to P5 are located at the top of mining drift. See Fig. 5 for the exact location of the observation points.

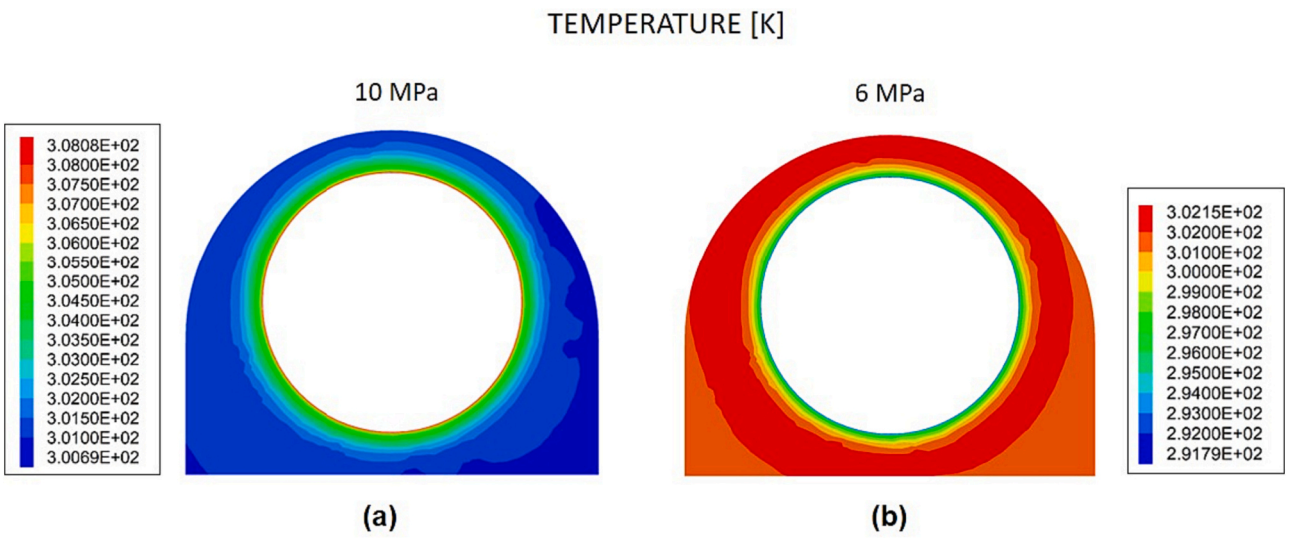

Fig. 15. Thermo-mechanical analysis. Temperature distribution in the sealing layer and concrete lining. (a) Maximum air temperature at 10 MPa; (b) minimum air temperature at 6 MPa.

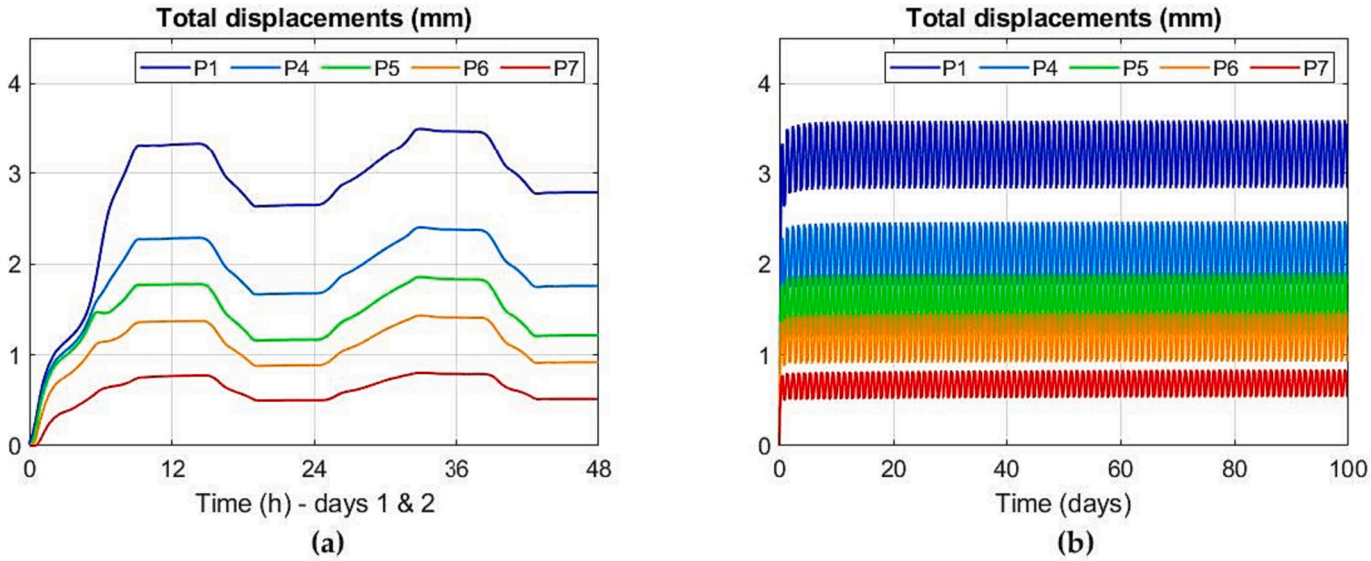

Fig. 16. Thermo-mechanical analysis. Total displacements in sealing layer, concrete lining and shale rock mass at the top of the drift. (a) First 48 h of operation; (b) 100 days of operation. P1 point is located in the sealing layer, P4 in the concrete lining and P6 and P7 points in the rock mass at the top of the mining drift. See Fig. 5 for exact locations of observation points.

Fig. 15, the results obtained also indicate a homogeneous temperature in other areas of the cross section (walls and floor).

Fig. 16 shows the total displacements at the top of the drift during the operation of the CAES system. Total displacements follow the air pressure. Fig. 16a presents the results for 48 h of operation and Fig. 16b indicate the results during 100 operation cycles. Maximum displacements reach 3.6 mm at P1 after 16 h of compression. Total displacements of 2.4 mm can be observed at point P4 (concrete lining). Regarding the deformation in the rock mass, displacements less than 1 mm are obtained (P7). The results show a very limited influence of the temperature on the stability compared to the effects of air pressure. As shown in Fig. 16b, the total displacements remain constant over 100 operating cycles.

Fig. 17 shows the total displacements in the concrete lining for different observation points. Due to the location of shale and sandstone, the deformation increases at the top and on the left wall of the drifts and decreases on floor and right wall. Displacements less than 1 mm are reached at points P9 and P14. Finally, the total displacements in shale, sandstone and coal seam, are presented in Fig. 18. Displacements less than 0.6 mm can be observed in sandstone (P10 and P16) increasing up to 1.4 and 2.1 mm in shales at P6 and P20, respectively.

Maximum and minimum principal stresses are depicted in Fig. 19 at the concrete lining for the monitoring points P4 and P9 at the top and right wall of the drift, respectively. Fig. 19a represents the evolution of the principal stresses after two operation cycles.

Note that the maximum principal stress (= least major compressive or even tensile stress) at points P4 and P9 follows the air pressure. The maximum principal stress in the charging stage at point P4 increases rapidly reaching a tensile stress of 9.5 MPa. The tensile stress reaches 4.6 MPa at point P9 at the right wall, where the sandstone is located. The minor principle stresses at points P4 and P9 fluctuate between −2.8 MPa and −3.7 MPa and between −5.1 MPa and −7.8 MPa, respectively, during the CAES operation. Please note: Due to the sign convention, negative values indicate compressive stresses and positive values tensile

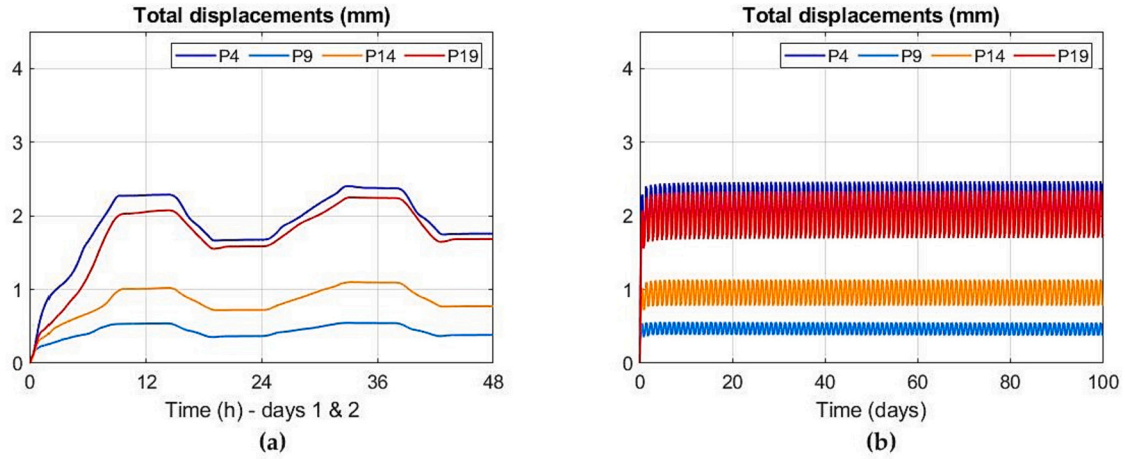

Fig. 17. Thermo-mechanical analysis. Total displacements at concrete lining. (a) First 48 h of operation; (b) 100 days of operation. P4, P9, P14 and P19 points are located in the concrete lining at top, right wall, floor and left wall of the mining drift. See Fig. 5 for exact location of observation points.

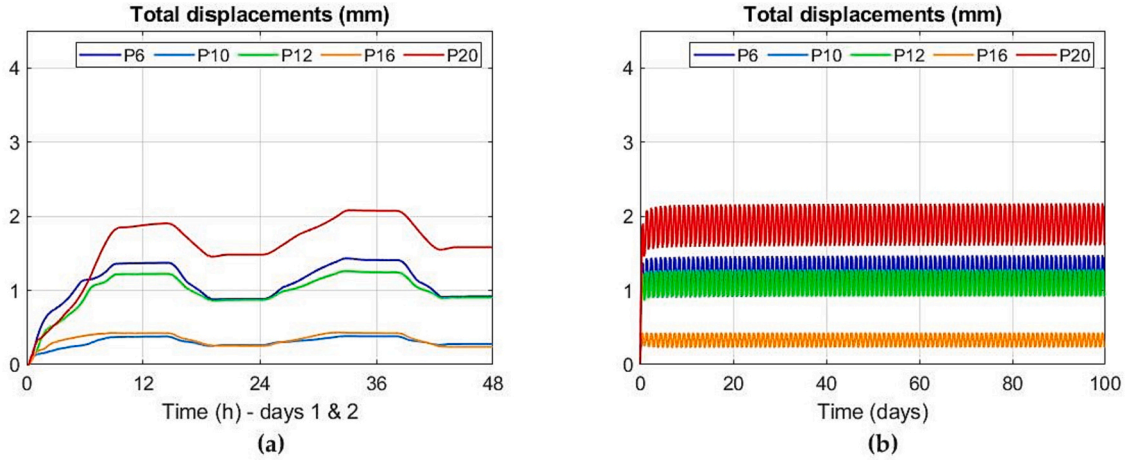

Fig. 18. Thermo-mechanical analysis. Total displacements at shale, sandstone and coal seam. (a) First 48 h of operation; (b) 100 days of operation. See Fig. 5 for exact location of observation points.

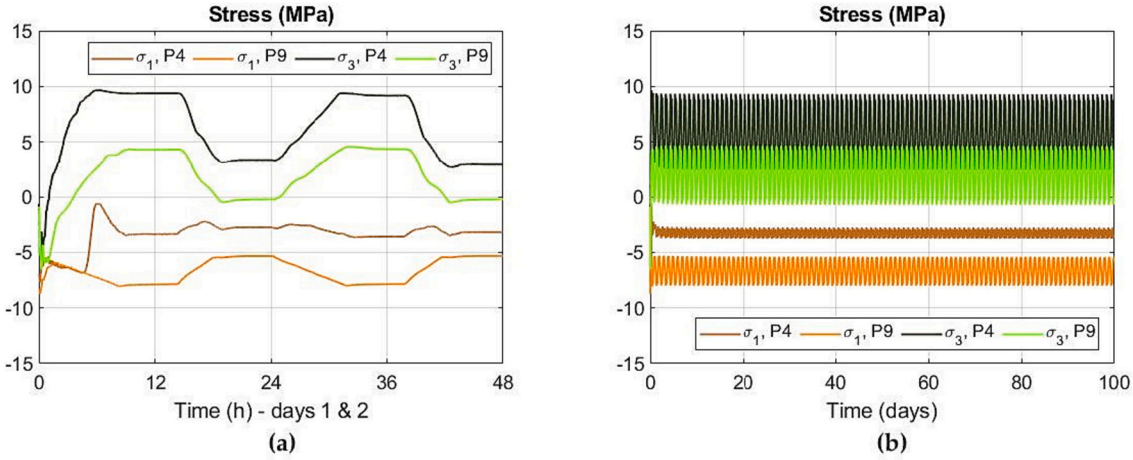

Fig. 19. Thermo-mechanical analysis. Maximum and minimum principal stresses in the concrete lining (P4 and P9) at the top of the drift. (a) First 48 h of operation; (b) 100 days of operation. See Fig. 5 for exact location of observation points P4 and P9.

stresses.

Maximum displacements and maximum principal stresses in the concrete lining during the CAES operation are shown in Fig. 20. The maximum displacements reach 3.61 mm and occur at the top and left wall of the drift, where shale and coal seam are located. As shown in Fig. 20b, the tensile stress reaches 9.5 MPa in a thickness of

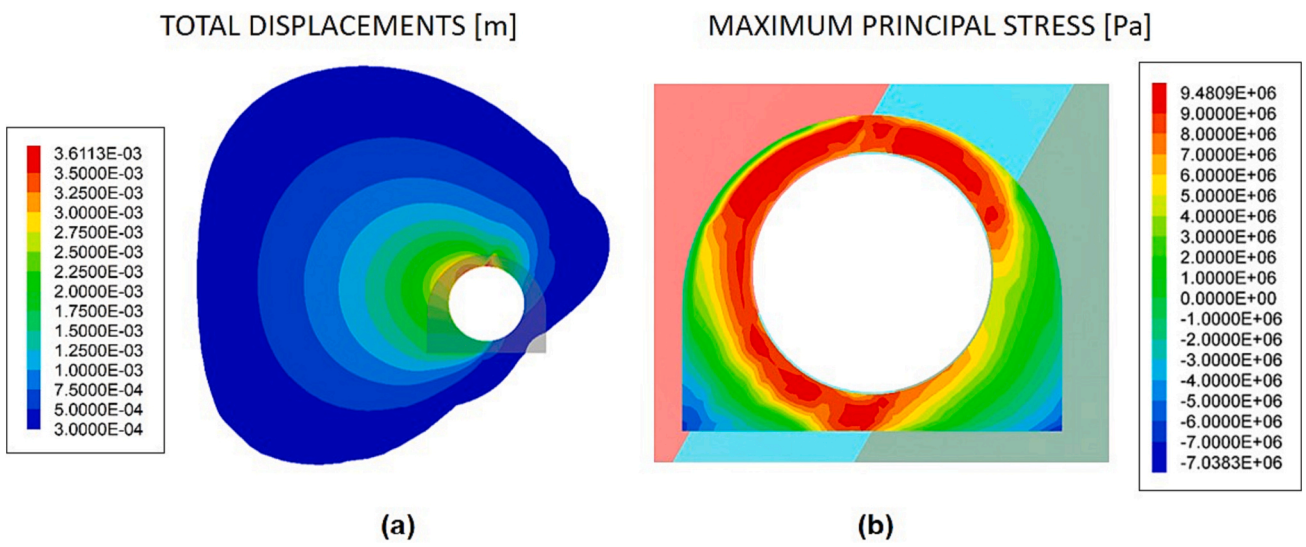

Fig. 20. Thermo-mechanical analysis. (a) Total displacements observed during the operation; (b) maximum principal stress in the concrete lining.

approximately 0.3 m at the top, floor and left wall of the drift. A suitable reinforcement in the concrete should be applied in those areas, where the maximum values of tensile stress are observed during the operation. The tensile stress decreases in the right wall, mainly due to the presence of sandstone. Note that at the bottom corners of the concrete lining the maximum principal stress is negative, indicating that these areas are under compression (compressive stress values up to 7 MPa are reached).

4. Conclusions

The stability of lined mining drifts as an underground reservoir of CAES systems is investigated. Four levels in a closed coal mine with three different variants of concrete lining are considered. A numerical model has been conducted to determine the most appropriate mining level and concrete lining. Air pressures of 6, 10, 20 and 25 MPa are applied considering the three variants of concrete lining with a minimum thickness of 0.35 m. In order to understand the behavior of the system, the openings are submitted to extreme pressures (much higher than the operating pressure). The results obtained indicate that lower deformations and tensile stresses in the concrete lining are reached at levels 1 and 3 employing an inner circular concrete lining. Due to the length of available drifts and state of conservation, level 3 is selected to analyze the coupled thermo-mechanical behavior of the lined drifts during the operation of the CAES system. At level 3, the mining drifts follow the coal seam with shale on top and sandstone at the bottom of the coal seam. The use of the horseshoe-shaped concrete lining implies less concrete and length of mining roadways to reach the useful volume of 68,000 m^3, reducing the investment costs. However, according to the results obtained, due to the tensile stress evolution and larger total displacements reached in the concrete lining this cross section is critical. Therefore, a technical feasibility could be achieved using a circular concrete lining.

Therefore, to investigate the stability of level 3, a more detailed thermo-mechanical numerical model is established considering cyclic loading with air pressures from 6 to 10 MPa and circular concrete lining with a 20 mm thick sealing layer on the inner face of the concrete. In order to determine the boundary conditions of the numerical model, a one-dimensional model is developed to predict the evolution of the air temperature and pressure inside the reservoir for 100 operation cycles. With the materials and operating conditions considered for the CAES plant, the evolution of the temperature field and total displacements remain constant and no additional cycles are required to investigate the coupled thermo-mechanical performance during the operation.

The obtained results show that slight temperature fluctuations are observed in the sealing layer and concrete lining and temperature variations in the rock mass are insignificant. Therefore, a very limited influence of the temperature on the stability compared to the effects of air pressure is observed. However, the temperature field depends on the capacity of the reservoir, operating conditions (air mass flow rates and air inlet temperature) and thermal properties of the materials, mainly thermal conductivity. When the air inlet temperature and the air mass flow rate increase, the charging period is reduced and the temperature field varies, reaching the rock mass. The maximum tensile stress reached 9.5 MPa in the concrete lining decreasing at the right wall, where the sandstone rock mass is located. Total displacements reached 3.6 mm at a pressure inside the reservoir of 10 MPa at the top of the mine drift. However, lower deformations are obtained at the floor and right wall. Tensile stresses and deformations remain constant during the long-term operation of the CAES system. Finally, the technical feasibility of the underground reservoir in lined mine drifts can be achieved for the operating conditions considered using a circular concrete lining with a suitable reinforcement in the concrete lining to resist the tensile and compressive stresses. Note, that thermo-mechanical cyclic fatigue effects are not yet considered, but they are important for any long-term considerations, lifetime and maintenance.

CRediT authorship contribution statement

Falko Schmidt: Conceptualization, Methodology, Software, Investigation, Writing – original draft, Writing – review & editing, Visualization. **Javier Menéndez:** Conceptualization, Methodology, Software, Investigation, Writing – original draft, Writing – review & editing, Visualization, Supervision. **Heinz Konietzky:** Conceptualization, Methodology, Writing – review & editing, Supervision. **Zhongming Jiang:** Conceptualization, Methodology, Supervision. **Jesús M. Fernández-Oro:** Conceptualization, Methodology, Software, Investigation, Validation. **Laura Álvarez:** Conceptualization, Validation, Supervision. **Antonio Bernardo-Sánchez:** Conceptualization, Validation, Supervision.

Declaration of competing interest

The authors declare that they have no known competing financial interests or personal relationships that could have appeared to influence the work reported in this paper.

Data availability

Data will be made available on request.

References

[1] BP, Statistical review of world energy. https://www.bp.com/en/global/corporate/energy-economics/statistical-review-of-world-energy.html. Accessed on 25/05/2023.

[2] F. Winde, F. Kaiser, E. Erasmus, Exploring the use of deep level gold mines in South Africa for underground pumped hydroelectric energy storage schemes, Renew. Sustain. Energy Rev. 78 (2016) 668–682.

[3] A.B. Gallo, J.R. Simões-Moreira, H. Costa, M.M. Santos, E. Moutinho dos Santos, Energy storage in the energy transition context: a technology review, Renew. Sustain. Energy Rev. 65 (2016) 800–822.

[4] J. Menéndez, F. Schmidt, H. Konietzky, J.M. Fernández-Oro, M. Galdo, J. Loredo, M.B. Díaz-Aguado, Stability analysis of the underground infrastructure for pumped storage hydropower plants in closed coal mines, Tunn. Undergr. Space Technol. 94 (2019), 103117.

[5] J. Menéndez, F. Schmidt, H. Konietzky, A.B. Sánchez, J. Loredo, Empirical analysis and geomechanical modelling of an underground water reservoir for hydroelectric power plants, Appl. Sci. 10 (2020) 5853, https://doi.org/10.3390/app10175853.

[6] X. Luo, J. Wang, M. Dooner, J. Clarke, Overview of current development in electrical energy storage technologies and the application potential in power system operation, Appl. Energy 137 (2015) 511–536.

[7] L. Geissbühler, V. Becattini, G. Zanganeh, S. Zavattoni, M. Barbato, A. Haselbacher, A. Steinfeld, Pilot-scale demonstration of advanced adiabatic compressed air energy storage, part 1: plant description and tests with sensible thermal-energy storage, J. Energy Storage 17 (2018) 129–139.

[8] V. Becattini, L. Geissbühler, G. Zanganeh, A. Haselbacher, A. Steinfeld, Pilot-scale demonstration of advanced adiabatic compressed air energy storage, part 2: tests with combined sensible/latent thermal-energy storage, J. Energy Storage 17 (2018) 140–152.

[9] C. Desai, A. Varadarajan, A constitutive model for quasi-static behavior of rock salt, J. Geophys. Res. 92 (1987) 445–456.

[10] K. Fuenkajorn, S. Serata, Numerical simulation of strain — softening and dilation of rock salt, Int. J. Rock Mech. Min. Sci. 30 (7) (1993) 1303–1306.

[11] S. Heusermann, O. Rolfs, U. Schmidt, Nonlinear finite element analysis of solution mined storage caverns in rock salt using the LUBBY2 constitutive model, Comput. Struct. 81 (2003) 629–638.

[12] Z. Hou, Mechanical and hydraulic behavior of rock salt in the excavation disturbed zone around underground facilities, Int. J. Rock Mech. Min. Sci. 40 (2003) 725–738.

[13] F. Crotogino, K.-U. Mohmeyer, R. Scharf, Huntorf CAES: More than 20 Years of Successful Operation. Orlando, Florida, USA, 2001.

[14] S. Succar, R.H. Williams, Compressed air energy storage: theory, resources, and applications for wind power, in: Princeton Environmental Institute Report, 2008, p. 8.

[15] W. He, X. Luo, D. Evans, J. Busby, S. Garvey, D. Parkes, J. Wang, Exergy storage of compressed air in cavern and cavern volume estimation of the large-scale compressed air energy storage system, Appl. Energy 208 (2017) 745–757.

[16] M. Nakhamkin, L. Andersson, E. Swensen, J. Howard, R. Meyer, R. Schainker, et al., AEC 110 MW CAES plant: status of project, J. Eng. Gas Turbines Power 114 (1992) 695–700.

[17] V. Tola, V. Meloni, F. Spadaccini, G. Cau, Performance assessment of Adiabatic Compressed Air Energy Storage (A-CAES) power plants integrated with packed-bed thermocline storage systems, Energ. Conver. Manage. 151 (2017) 343–356.

[18] M. Lutyński, An overview of potential benefits and limitations of Compressed Air Energy Storage in abandoned coal mines, IOP Conf. Ser. Mater. Sci. Eng. 268 (2017), 012006.

[19] H. Ibrahim, A. Ilinca, J. Perron, Energy storage systems—characteristics and comparisons, Renew. Sustain. Energy Rev. 12 (2008) 1221–1250.

[20] T. Ishihata, Underground compressed air storage facility for CAES-G/T power plant utilizing an airtight lining, News J. Int. Soc. Rock Mech. 5 (1) (1997) 17–21.

[21] A. Pudewills, J. Droste, Numerical modeling of the thermomechanical behavior of a large-scale underground experiment, Comput. Struct. 81 (8–11) (2003) 911–918.

[22] K. Serbin, J. Slizowski, K. Urbanczyk, S. Nagy, The influence of thermodynamic effects on gas storage cavern convergence, Int. J. Rock Mech. Min. Sci. 79 (2015) 166–171.

[23] M. Nakata, H. Yamachi, A. Nakayama, S. Sakurai, T. Shidahara, Thermodynamical approach to compressed air energy storage system, Doboku Gakkai Ronbunshu 610 (1998) 31–42.

[24] J. Rutqvist, H.-M. Kim, D.-W. Ryu, J.-H. Synn, W.-K. Song, Modeling of coupled thermodynamic and geomechanical performance of underground compressed air energy storage in lined rock caverns, Int. J. Rock Mech. Min. Sci. 52 (2012) 71–81.

[25] K. Khaledi, E. Mahmoudi, M. Datcheva, T. Schanz, Analysis of compressed air storage caverns in rock salt considering thermomechanical cyclic loading, Environ. Earth Sci. 75 (2016) 1149.

[26] K. Khaledi, E. Mahmoudi, M. Datcheva, T. Schanz, Stability and serviceability of underground energy storage caverns in rock salt subjected to mechanical cyclic loading, Int. J. Rock Mech. Min. Sci. 86 (2016) 115–131.

[27] B. Damjanac, C. Carranza-Torres, R. Dexter, Technical Review of the Lined Rock Caverns (LRC) Concept and Design Methodology: Steel Liner Response, Itasca Consulting Group, Inc., Minneapolis, Minnesota, 2002.

[28] J. Johansson, High Pressure Storage of Gas in Lined Rock Caverns and Cavern Wall Design Principles, Licentiate Thesis., Division of Soil & Rock Mechanics, Royal Institute of Technology, Stockholm, Sweden, 2003.

[29] P. Perazzelli, G. Anagnostou, J. Amberg, Uplift analysis for CAES tunnels, in: The 14th International Conference of the International Association for Computer Methods and Advances in Geomechanics, CRC Press, Kyoto, 2014, pp. 1691–1696.

[30] H. Konietzky, X. Li, and W. Chen Lifetime prediction of rocks chapter 19, Shen et al. (eds.), Modelling Rock Fracturing Processes.

[31] S. Zhou, C. Xia, H. Zhao, S. Mei, Y. Zhou, Numerical simulation for the coupled thermo-mechanical performance of a lined rock cavern for underground compressed air energy storage, J. Geophys. Eng. 14 (2017) 1382–1398 (17 pp).

[32] D. Parkes, D.J. Evans, P. Williamson, J.D.O. Williams, Estimating available salt volume for potential CAES development: a case study using the Northwich Halite of the Cheshire Basin, J. Energy Storage 18 (2018) 50–61.

[33] F. Schmidt, J. Menéndez, H. Konietzky, P. Pascual-Muñoz, J. Castro, J. Loredo, A. B. Sánchez, Converting closed mines into giant batteries: effects of cyclic loading on the geomechanical performance of underground compressed air energy storage systems, J. Energy Storage 32 (2020), 101882.

[34] L. Alvarez, J. Menendez, A. Bernardo-Sanchez, M. Galdo, J. Loredo, J. M. Fernandez-Oro, Thermodynamic analysis of compressed air energy storage (CAES) reservoirs in abandoned mines using different sealing layers, Appl. Sci. 11 (2021) 2573.

[35] J. Menendez, J.M. Fernandez-Oro, M. Galdo, L. Alvarez, A. Bernardo-Sanchez, Numerical investigation of underground reservoirs in compressed air energy storage systems considering different operating conditions: influence of thermodynamic performance on the energy balance and round-trip efficiency, J. Energy Storage 46 (2022), 103816.

[36] H. Kim, J. Rutqvist, H. Kim, D. Park, D. Ryu, E. Park, Failure monitoring and leakage detection for underground storage of compressed air energy in lined rock caverns, Rock Mech. Rock. Eng. 49 (2016) (2016) 573–584.

[37] H. Kim, J. Rutqvist, J. Jeong, B. Choi, D. Ryu, W. Song, Characterizing excavation damaged zone and stability of pressurized lined rock caverns for underground compressed air energy storage, Rock Mech. Rock Eng. 46 (2013) 1113–1124.

[38] X. Chen, J.G. Wang, Stability analysis for compressed air energy storage cavern with initial excavation damage zone in an abandoned mining tunnel, J. Energy Storage 45 (2022), 103725.

[39] Y. Xu, S. Zhou, C. Xia, H. Zhao, X. Xue, Three-dimensional thermo-mechanical analysis of abandoned mine drifts for underground compressed air energy storage: a comparative study of two construction and plugging schemes, J. Energy Storage 39 (2021), 102696.

[40] D. Wu, J.G. Wang, B. Hu, S. Yang, A coupled thermo-hydro-mechanical model for evaluating air leakage from an unlined compressed air energy storage cavern, Renew. Energy 146 (2020) 907–920.

[41] Z. Jiang, P. Li, D. Tang, H. Zhao, Y. Li, Experimental and numerical investigations of small-scale lined rock cavern at shallow depth for compressed air energy storage, Rock Mech. Rock Eng. 53 (2020) 2671–2683.

[42] J. Menéndez, J. Loredo, L. Álvarez, J.M. Fernández-Oro, A. Bernardo-Sánchez, Analytical models for adiabatic compressed air energy storage (A-CAES) systems in lined tunnels, IOP Conf. Ser. Earth Environ. Sci. 897 (2021), 012008.

[43] M. Zeynalian, A.H. Hajialirezaei, A.R. Razmi, M. Torabi, Carbon dioxide capture from compressed air energy storage system, Appl. Therm. Eng. 178 (2020), 115593.

[44] A.R. Razmi, M. Janbaz, Exergoeconomic assessment with reliability consideration of a green cogeneration system based on compressed air energy storage (CAES), Energ. Conver. Manage. 204 (2017), 112320.

[45] S.M. Alirahmi, A.R. Razmi, Ahmad Arabkoohsar, Comprehensive assessment and multi-objective optimization of a green concept based on a combination of hydrogen and compressed air energy storage (CAES) systems, Renew. Sustain. Energy Rev. 142 (2021), 110850.

[46] A.R. Razmi, M. Soltani, A. Ardehali, K. Gharali, M.B. Dusseault, J. Nathwani, Design, thermodynamic, and wind assessments of a compressed air energy storage (CAES) integrated with two adjacent wind farms: a case study at Abhar and Kahak sites, Iran, Energy 221 (2021), 119902.

[47] A.R. Razmi, H.H. Afshar, A. Pourahmadiyan, M. Torabi, Investigation of a combined heat and power (CHP) system based on biomass and compressed air energy storage (CAES), Sust. Energy Technol. Assess. 46 (2021), 101253.

[48] L. Kuang, Q, Zhu, J, Wang, Bo Wang., On a possible mechanism of hydrostatic pressure on mineshaft linings in Western China, Geofluids (2022) 4090878.

[49] X. Lyu, T. Zhang, L. Yuan, K. Yang, J. Fang, S. Li, S. Liu, Pumped storage hydropower in abandoned mine shafts: key concerns and research directions, Sustainability 14 (2022) 1601.

[50] R. Kushnir, A. Dayan, A. Ullmann, Temperature and pressure variations within compressed air energy storage caverns, Int. J. Heat Mass Transf. 55 (2012) 5616–5630.

[51] Itasca, FLAC3D. Fast Lagrangian Analysis of Continua in 3 Dimensions, Version 7.0. Minneapolis: Itasca Consulting Group.

[52] ISRM, Rock Characterization, Testing and Monitoring, ISRM Suggested Method, International Society for Rock Mechanics. Pergamon Press, Oxford, In, 1981.

[53] Hoek E, Carranza-Torres C and Corkum B., 2002. Hoek-Brown failure criterion – 2002 edition, Proc. NARMS-TAC Conference, Toronto. 1, 267–273.

[54] S. Zhou, C. Xia, S. Du, P. Zhang, Y. Zhou, An analytical solution for mechanical responses induced by temperature and air pressure in a lined rock cavern for underground compressed air energy storage, Rock Mech. Rock Eng. 48 (2015) 749–770.